Wavelet packet-based digital relaying for advanced series compensated line

S.R. Samantaray and P.K. Dash

Abstract: A new approach for the protection of thyristor-controlled series-compensated (TCSC) line using wavelet packets transform (WPT) is presented. The proposed method uses one cycle post-fault-current samples just after fault inception, which is processed through WPT and decomposed into various decomposition levels. The decomposed components are grouped together to provide different frequency sub-bands. Then the phase selection signal (PSS) and section identification signal (SIS) are computed to identify the faulty phase and faulty section, respectively, involved in the fault process in transmission line including TCSC. A threshold value (THD) is selected for PSS, and PSS above THD describes the faulty phase involved, otherwise not. Similarly, another THD is selected for SIS, and SIS below THD describes fault that includes TCSC, otherwise fault that does not include TCSC. As PSS takes half cycle after fault inception to identify the faulty phase and then triggers SIS, the faulty phases and faulty sections are identified within one cycle of fault inception. The proposed WPT algorithm is also tested on physical transmission line model with TCSC, under wide variations in operating conditions and provides accurate results. Thus, the proposed method provides accurate and fast protection measures for TCSC-based line.

1 Introduction

Use of FACTS devices to improve the power transfer capability in high voltage transmission line is of greater interest in these days. Thyristor-controlled series-compensated (TCSC) line [1–3] is one of the main FACTS devices, which has the ability to improve the utilisation of the existing transmission system. TCSC-based compensation possess thyristor-controlled variable capacitor protected by metal oxide varistor (MOV) and an air gap. The presence of the TCSC in fault loop not only affects the transient components but also the steady-state components. Significant differences exist between fault signals in presence of capacitor–MOV combination for faults encountering TCSC and not encountering TCSC. When the fault loop does not include TCSC, like an ordinary transmission line, the current signal of the relay contains decaying dc and high-frequency components besides fundamental frequency component. Thus, the apparent impedance calculations are similar to ordinary transmission lines. On the other hand, if the fault loop includes TCSC, the current signal consists of non-fundamental decaying frequency components, odd harmonics, high-frequency and the fundamental frequency components, and the apparent impedance calculations should account for the impedances introduced by TCSC and MOV combination. Thus, implementation of this technology changes the apparent line impedance, which is controlled by the firing angle of thyristors, and is accentuated by other factors including the MOV. The controllable reactance, the MOVs, protecting the capacitors and the air-gaps operation make the protection decision more complex and therefore conventional relaying scheme based on fixed settings has its limitation. Also, in series-compensated transmission lines equipped with MOV, the load current level may be of the order of the fault current towards the boundary of the zone which, in turn, affects the reach characteristics of the conventional distance relay. Further, the current level may be of the same order at two different points of the transmission line (before and after TCSC) for the similar type of fault. Thus, fault classification and fault section identification are very challenging tasks for a transmission line with TCSC.

Once the fault is classified, then its location relative to TCSC (fault section) is required to be determined. As the impedance calculations are different for fault encountering TCSC and not encountering TCSC, the fault section identification information is required to calculate the apparent impedance of the line accurately for different faulted conditions. If the fault does not include TCSC, then the impedance calculation is like ordinary transmission line, and when the fault includes TCSC, then the impedance calculation accounts for the impedances introduced by TCSC and MOV combination. The line impedance is compared with the protective zone and if the line impedance is less then the relay setting, then the relay gives a signal to trip the circuit breaker. Thus, before impedance calculation, a more reliable and accurate fault classification and fault section identification approach is necessary.

Different attempts have been made for fault classification and fault location determination using wavelet transform, Kalman filtering approach and neural network [1–11]. Neural network-based phase selection procedures [4, 5] are proposed which need large training set generation, longer training time and design of a new neural network for each transmission system. Further, such designs do not consider the presence of TCSC at midpoint of a line.

doi:10.1049/iet-gtd:20070052

Paper first received 13th October 2006 and in revised form 30th January 2007

S.R. Samantaray is with National Institute of Technology, Rourkela, India

P.K. Dash is with Centre for Research in Electrical, Electronics and Computer Engineering, Bhubaneswar, India

E-mail: sbh_samant@yahoo.co.in

Recently, wavelet transform is proposed as a new tool to power system area for power quality monitoring [8], data compression [9] and transient analysis [10, 11] using its multi-resolution feature and frequency and time domain analysis capability. Liao and Elangovan [13] proposed wavelet-based phase selection of an ordinary transmission line using the fault noise as signal which needs additional arrangement of stack tuner, and so on. In another attempt, Yu and Song [14] used wavelet integrated with neural network for phase selection for auto-reclosing purpose of an ordinary transmission line. Morlet wavelet is utilised to detect high impedance fault (HIF) and to distinguish HIF from switching events [15].

The Kalman filtering approach [1] finds its limitation, as fault resistance cannot be modelled and further it requires a number of different filters to accomplish the task. Back propagation neural network (BPNN), radial basis function neural network (RBFNN) and Fuzzy neural network (FNN) are employed for adaptive protection of such a line where the protection philosophy is viewed as a pattern classification problem. The networks generate the trip or block signals using a data window of voltages and currents at the relaying point. However, the above approaches are sensitive to system frequency changes, and require large training sets and training time and a large number of neurons.

This paper presents a new approach for fault classification and section identification of TCSC-based line using wavelet packet transform (WPT) [16–23] algorithm. In case of TCSC based line, there may be some situations where fault current levels may be smaller than the current at the loading condition. In such condition, the conventional protection scheme based on amplitude of current magnitude may fail to provide correct fault classification and section identification. Hence, it is required to extract features of the frequency components rather than magnitudes as higher harmonic components are pronounced because of the presence of TCSC. This is done by decomposing the signal into various sub-bands using WPT. The proposed scheme works on the assumption that the fault has been detected. The pre- and post-fault boundaries are detected using the fault detector that uses a short data window (four samples) algorithm [12]. The final indication of the fault is given only when three consecutive comparisons give the difference more than a specified threshold value (THD). Basically, WPT is ideal to extract features as a result of signal decomposition. Here, the fault current signal is decomposed into several frequency bands of high- and low-pass filters. In WPT, the signal is decomposed into both high- and low-pass components, whereas in the case of wavelet transform, only low-pass components are decomposed further. From the decomposed levels, phase selection signal (PSS) and selection indentification signal (SIS) are computed to provide the faulty phase and faulty section accordingly. The PSS detects the faulty phase within half cycles of fault inception and after that it triggers SIS to identify the faulty section involved in the fault process.

The current signals for all phases are retrieved at the relaying end at a sampling frequency of 1.6 kHz. The fault current is decomposed into five levels, which generate 32 uniform sub-bands of 25 Hz width. These sub-ands are grouped to provide harmonic groups, with each harmonic component in the centre of each band and with uniform 50 Hz interval. From the WPT coefficients of different bands, PSS and SIS are calculated to provide the information regarding the faulty phase and the faulty section involved. The WPT is an extension of (fast wavelet transform (FWT)) that allows for finer characterisation of signal content for both time and frequency together. The wavelet packets are more sensitive and computationally more flexible way to do signal discrimination than FFT- or FWT-based methods.

2 Wavelet packets

2.1 Discrete wavelet transform

The discrete wavelet transform is briefly discussed that is needed for definitions of wavelet packets. The wavelet scaling function and mother wavelets are functions that satisfy the following two-scale equations (n is an integer)

$$\phi(t) = \sqrt{2}\sum_n h_n \phi(2t-n) \tag{1}$$

$$\psi(t) = \sqrt{2}\sum_n g_n \phi(2t-n) \tag{2}$$

for some set of coefficients $H = \{h_n\}$ and $G = \{g_n\}$ for which $g_n = (-1)h_{1-n}$. That is, G is the reverse of H, interleaved with sign changes. Each wavelet scaling function and mother wavelet function is represented by a set of coefficients H and G. The coefficients $H = \{h_n\}$ and $G = \{g_n\}$ are low pass and high pass filter coefficients, respectively. They are used to construct the set of wavelet basis functions $\phi_{jk}(t)$ and $\psi_{jk}(t)$, defined below; these are scaled and translated copies of the scaling function $\phi(t)$ and the mother wavelet $\psi(t)$.

$$\phi_{jk}(t) = 2^{-j/2}\phi(2^{-j}t-k) \tag{3}$$

$$\psi_{jk}(t) = 2^{-j/2}\psi(2^{-j}t-k) \tag{4}$$

If j and k are integers, then the basis functions are scaled by a factor of 2^j, and translated k time units. If the time resolution of a discretely sampled function is Δt, then $\phi_{jk}(t)$ or $\psi_{jk}(t)$ is the same as $\phi_{j0}(t-\Delta t)$ or $\psi_{j0}(t-k\Delta t)$.

Now for $i(t)$, a signal of length 2^N, then there is maximum N level of decomposition and wavelet transform decomposition of $i(t)$ can be given as

$$i(t) = \sum_{k=0}^{2^{N-j-1}} a_{jk}\phi_{jk}(t) + \sum_{j=1}^{J}\sum_{k=0}^{2^{N-j-1}} d_{jk}\psi_{jk}(t) \tag{5}$$

2.2 Wavelet packet transform

Here, in the case of wavelet packets [16], the sub-band information represented by the detail coefficients $\{d_{jk}\}$ can be decomposed further. The advantage of this further series of operations is that the time frequency plane is partitioned more precisely; in fact, the filtering sequence can be adjusted even further in order to represent the signal energy more efficiently onto a minimal number of non-zero coefficients, which has obvious advantages in signal compression. If we have a signal $i(t)$ of length 2^N, then for J levels of decomposition, we have 2^J sets of sub-band coefficients of length 2^{N-j}. Each set is a downsampled, band-pass filtered copy of the $i(t)$ as with regular wavelets, but with more resolution in time.

Wavelet packets are then generalisations of wavelets. Let $m = 0$ to $2^j - 1$, where J is being defined earlier as the depth of the filtering tree or number of levels of decomposition. Let us define the even and odd wavelet packets $W_{2m}(t)$ and $W_{2m+1}(t)$ as with wavelets in (1) and (2) by

$$W_{2m}(t) = \sqrt{2}\sum_n h_n W_m(2t-n) \tag{6}$$

and

$$W_{2m+1}(t) = \sqrt{2}\sum_n g_n W_m(2t-n) \tag{7}$$

Using this notation, $\phi(t) = W_0(t)$ and $\psi(t) = W_1(t)$. Since wavelet packets are generalisations of wavelets, then a series of basis functions $W_{jmk}(t)$ can be generated by scaled and translated versions of $W_m(t)$ as in (3) and (4).

$$W_{jmk}(t) = 2^{-j/2} W_m(2^{-j}t - k) \tag{8}$$

In a wavelet packet analysis, a signal $i(t)$ is represented as sum of orthogonal wavelet packet functions $W_{jmk}(t)$ at different scales, oscillations and locations

$$i(t) = \sum_j \sum_m \sum_k w_{jmk} W_{jmk}(t) \tag{9}$$

where w_{jmk} is the wavelet packet coefficient.

The wavelet packet decomposition tree is shown in Fig. 1. It generates 32 sub-bands of coefficients comprising m_1 through m_{32}. Then, these sub-ands are grouped to provide harmonic groups, with each harmonic component in the centre of each band and with uniform 50 Hz interval, generating different frequency bands, $d_1(k)$ through $d_{15}(k)$. The choice of mother wavelet plays a significant role in detecting and localising different types of fault transients. In addition to this, the choice also depends on particular application. In this study, we are interested in detecting and analysing short duration, fast decaying and oscillating type of high-frequency current signals. One of the popular wavelets suitable for such application (power system transients) is Daubichies's wavelet. Thus, in this paper, db1 is used to extract features at specific level of decomposition.

3 System studied

A 400-kV, 50-Hz power system is illustrated in Fig. 2. In this system, a TCSC is located at midpoint of the transmission line, used for the distance protection study. The power system consists of two sources: TCSC and associated components and a 300-km transmission line. The transmission line has zero sequence impedance $Z(0) = 96.45 + j335.26\ \Omega$ and positive sequence impedance $Z(1) = 9.78 + j110.23\ \Omega$. $E_s = 400\,\text{kV}$ and $E_R = 400\angle\delta\,\text{kV}$. Shunt capacitance $C(1) = 3.82\ \mu\text{F}$ and $C(0) = 2.32\ \mu\text{F}$. The TCSC is designed to provide compensation varying from 30% (minimum) to 40% (maximum). All

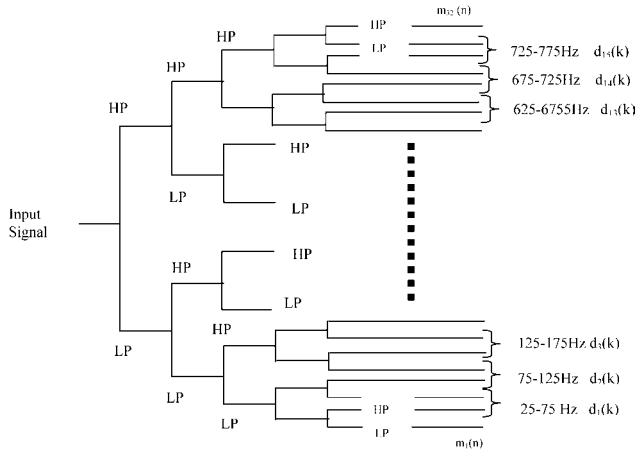

Fig. 1 *Wavelet packet decomposition tree and grouped sub-bands*

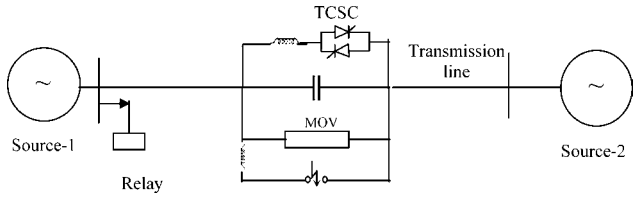

Fig. 2 *TCSC-based line*

the components are modelled using the EMTDC subroutines.

The MOV consists of a number of zinc oxide disks electrically connected in series and parallel. The purpose of the MOV is to prevent the voltage across the capacitor from rising to levels which will damage the capacitor. This is most likely to happen when a fault occurs at a point on the compensated line which minimizes the impedance of the fault loop. When instantaneous voltage across the capacitor approaches a dangerous level, the MOV begins to draw a significant proportion of the line current and thereby limiting the voltage across the capacitor at that level. This action alters the impedance in the series path and hence the fault-loop impedance. In the event that the MOV remains in conduction long enough to raise its temperature (energy) to a dangerous level an air-gap is triggered to short out both the MOV and the capacitor, again changing the fault loop impedance. The operation of the MOV can be within the first half cycle of fault and depending on the severity of the fault, it may continue to operate until the air-gap is triggered cycles later. This is precisely the time when a digital relay makes protection decision. Further, a bypass switch in parallel with the gap automatically closes for abnormal system conditions that cause prolonged current flow through the gap. Fig. 3*a* shows the MOV with air gap, discharge reactor and bypass switch and with MOV arrangement, and Fig. 3*b* shows the MOV voltage against current characteristics. Fig. 4 shows the fault current with TCSC at different firing angles and Fig. 5 shows the variations in fault current for fault before and after TCSC on the line. The small inductance in the arrangement limits the current through the air-gap or switch circuit. The TCSC is designed such that it provides 30% compensation at 180° (minimum) and 40% compensation at 150° (maximum) firing angle and in this study the firing angle is varied within this range as shown in Fig. 6.

The TCSC is placed at 50% of the transmission line with 300 km line length, which is 150 km from relaying end. The simulation for all 11 types of shunt faults (L-G,LL-G,LL,LLL,LLL-G) are made on the transmission line with different fault resistance, source impedance, incident angles at different fault locations with varying the firing angle from 150° to 180° with (after) and without including (before) TCSC. Fig. 6 provides the variation in capacitive reactance with firing angle.

4 Feature extraction and simulation result using WPT

4.1 Feature extraction

In the proposed method, the sampling rate chosen is 1.6 kHz and the fault current is decomposed to five levels, which generate 32 uniform sub-bands of 25 Hz width. The wavelet packet tree is developed using db1 wavelet function. The corresponding sub-bands resulted are $m_1(n)$ through $m_{32}(n)$. The $m_1(n)$ is of 0–25 Hz, $m_2(n)$ is of 25–50 Hz,

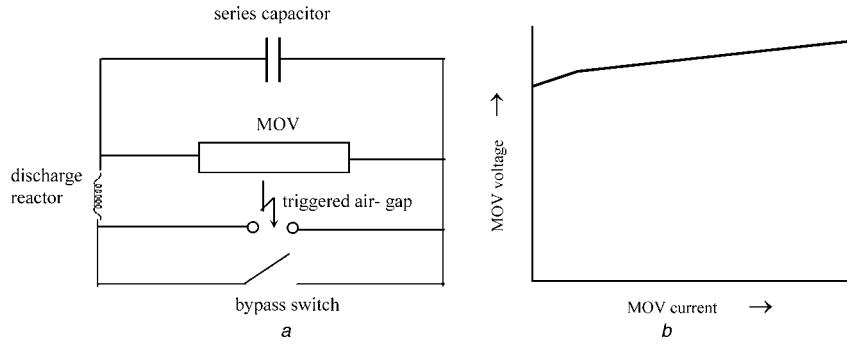

Fig. 3 *MOV arrangements and MOV voltage against current charecteristics*
a MOV protected series capacitor
b MOV characteristic

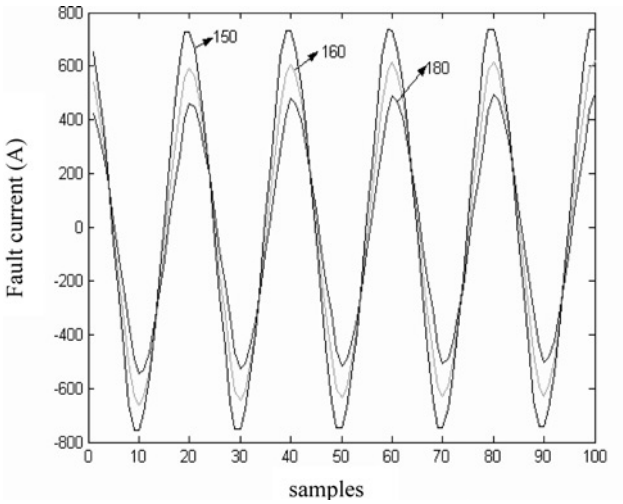

Fig. 4 *Fault current with TCSC at different firing angles*

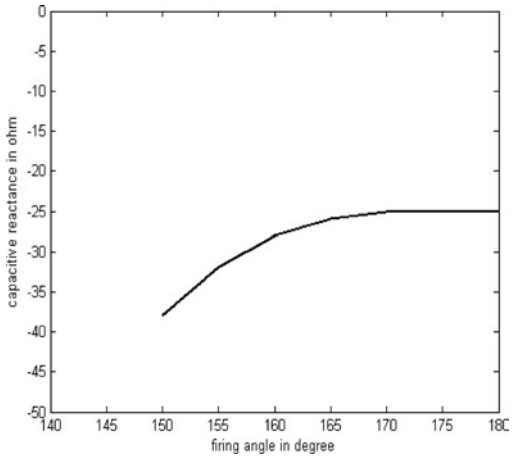

Fig. 6 *Variation of capacitive reactance with firing angle*

$m_3(n)$ is of 50–75 Hz and $m_{32}(n)$ is of 775–800 Hz. These sub-bands are grouped together to provide other frequency bands with required centre frequency. For example $m_2(n)$ and $m_3(n)$ are grouped together to provide $d_1(k)$, to form another band of frequency 25–75 Hz, where the centre frequency is 50 Hz and this band keeps the information regarding fundamental component. Similarly, $m_4(n)$ and $m_5(n)$ are grouped together to provide $d_2(k)$ of 75–125 Hz, where the centre frequency is 100 Hz. Thus, $d_1(k)$ through d_{15} (k) are formed to keep the information up to 775 Hz. These grouped WPT coefficients are used to find out the PSS and SIS for faulty phase and faulty section involved, respectively, as given in the following section. One cycle data after fault inception is processed through WPT to compute PSS and SIS.

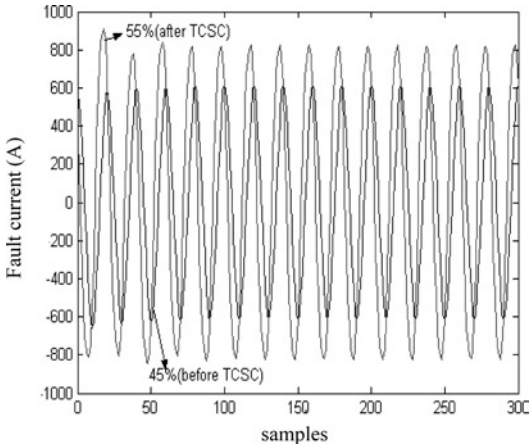

Fig. 5 *Fault current before and after TCSC at 160° firing angle*

4.2 Faulty phase selection

After feature extraction, the PSS was found out. The PSS is found out on the $d_1(k)$ information only which provides frequency band with centre frequency 50 Hz.

$$\mathrm{PSS}(k) = \sum_{k=1}^{n} |d_1(k)| \tag{10}$$

where k is the most recent sample and n is the number of samples in the window. Here the window length is taken as 3, that is consecutive three samples are taken. The PSS provides the information regarding the faulty phase involved. If the PSS moves above the selected THD, then that phase is considered to be faulty. Thus, the PSS is calculated with WPT band of 25–75 Hz which keeps the information around fundamental frequency as the centre frequency in $d_1(k)$ is 50 Hz.

Figs. 7*a–e* shows the PSS for faults at different operating conditions. Fig. 7*a* shows the PSS for abc-g fault at 20% of the line, firing angle $\alpha = 30^\circ$, fault resistance $R_f = 50\ \Omega$. THD was set at a value of 0.3 after testing the algorithm with wide variations in operating conditions. As the PSS is calculated on per unit (pu) scale, the selected THD is well suited for other operating conditions of the power system network. As seen in Fig. 7, for PSS above the

THD, the phases are involved in the fault. Similarly, Fig. 7*b* shows the PSS for abc-g fault at 40% of the line, $\alpha = 45^\circ$, $R_f = 100\ \Omega$ and Fig. 7*c* shows the PSS for abc fault at 60% of the line, $\alpha = 60^\circ$, $R_f = 150\ \Omega$ with 20% increase in source impedance.

Fig. 7*d* shows the PSS for ab-g fault at 75% of the line, $\alpha = 45^\circ$, $R_f = 200\ \Omega$, where for 'a' and 'b' phases, the PSS is above the THD, whereas for c-phase, the PSS is below the THD, showing 'a' and 'b' phases are faulty phases involved where as the c-phase is not involved in fault. Similarly, Fig. 7*e* shows the PSS for a–g fault at 95% of the line, $\alpha = 30^\circ$, $R_f = 200\ \Omega$.

As seen from the results that the PSS for the faults before and after the TCSC do not vary so much even if harmonics are generated for the faults incorporating TCSC because the PSS is calculated by taking only $d_1(k)$ which provides the features of low-frequency components (around fundamental frequency). Thus, a robust method for faulty phase selection

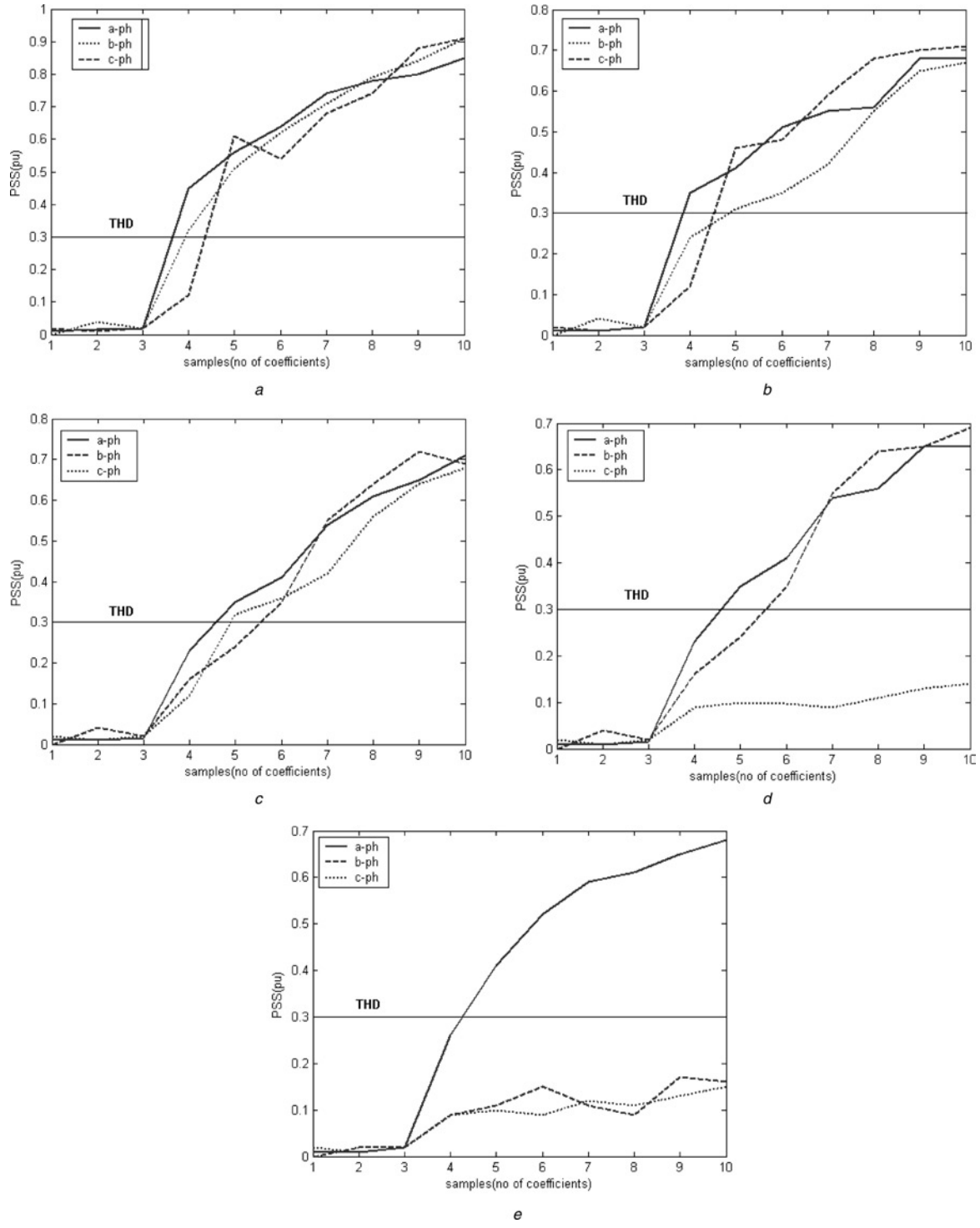

Fig. 7 *PSS for faults*

a PSS for abc–g fault at 20% of the line, $\alpha = 30^\circ$, $R_f = 50\ \Omega$
b PSS for 'abc–g' fault at 40% of the line, $\alpha = 45^\circ$, $R_f = 100\ \Omega$
c PSS for 'abc' fault at 60% of the line, $\alpha = 60^\circ$, $R_f = 150\ \Omega$, 20% increase in source impedance
d PSS for 'ab–g' fault at 75% of the line, $\alpha = 45^\circ$, $R_f = 200\ \Omega$
e PSS for 'a–g' fault at 95% of the line, $\alpha = 30^\circ$, $R_f = 200\ \Omega$

is proposed in this paper, which provides accurate results under different operating conditions.

4.3 Fault section identification

Fault section identification is required to find out whether the fault is with TCSC or without TCSC. The decomposed components can be considered as the features of the original signal. The sub-bands from $d_2(k)$ through $d_{15}(k)$ represent the level of higher frequency components which are pronounced in case of faults with TCSC. To distinguish the faulty section, the SIS is found out as per the following

$$\mathrm{SIS}(k) = \sum_{k=1}^{n} \left\{ |d_1 k| - \sum_{m=2}^{15} |d_m(k)| \right\} \tag{11}$$

where 'k' is the most recent sample and 'n' is the numbers of samples in the window considered. Here, in the proposed

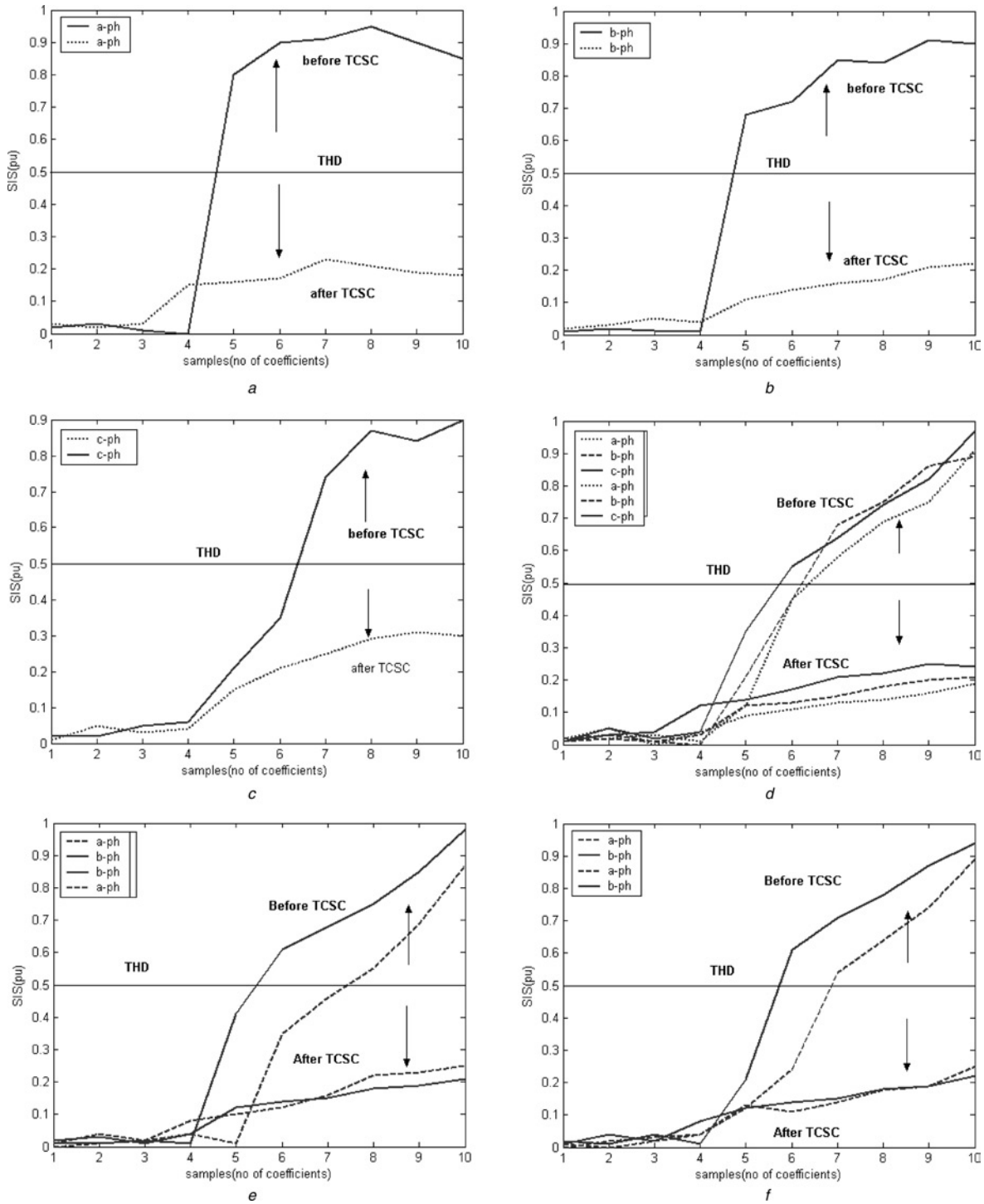

Fig. 8 *SIS computed for various fault conditions*

a SIS for a-ph in 'a–g' fault at 40% (before TCSC) and 60% (after TCSC) of the line, $\alpha = 30^\circ$, $R_f = 50\ \Omega$
b SIS for b-ph in 'b–g' fault at 30% (before TCSC) and 70% (after TCSC) of the line, $\alpha = 45^\circ$, $R_f = 75\ \Omega$
c SIS for c-ph in 'c–g' fault at 20% (before TCSC) and 60% (after TCSC) of the line, $\alpha = 60^\circ$, $R_f = 100\ \Omega$
d SIS for 'abc–g'-ph at 45% (before TCSC) and 65% (after TCSC) of the line, $\alpha = 45^\circ$, $R_f = 150\ \Omega$
e SIS for 'ab–g' fault at 15% (before TCSC) and 85% (after TCSC) of the line, $\alpha = 60^\circ$, $R_f = 100\ \Omega$
f SIS for 'ab' fault at 35% (before TCSC) and 75% (after TCSC) of the line, $\alpha = 30^\circ$, $R_f = 150\ \Omega$

method, the window length is taken as 3. Here, all the grouped bands are used in calculating SIS.

The SIS computed for various fault conditions are depicted in Figs. 8*a–f*. THD was set at a value of 0.5 after testing the algorithm with wide variations in operating conditions. As the SIS is calculated on per unit (pu) scale, the selected THD is well suited for other operating conditions of the power system network. Fig. 8*a* shows the SIS for a-ph in 'a–g' fault at 40% (before TCSC) and 60% (after TCSC) of the line, $\alpha = 30^{\circ}$, $R_f = 50\ \Omega$ and it is clearly seen that the SIS is much above the THD for fault before TCSC compared with SIS for the fault after the TCSC. Similarly, Fig. 8*b* and *c* shows the SIS for 'b–g' and 'c–g' fault respectively. Fig. 8*d* shows the SIS for 'abc–g' fault at 45% (before TCSC) and 65% (after TCSC) of the line, $\alpha = 45^{\circ}$, $R_f = 150\ \Omega$. In this case, SIS for all three phases before TCSC are above the THD compared to the SIS for all three phases after TCSC. Fig. 8*e* with

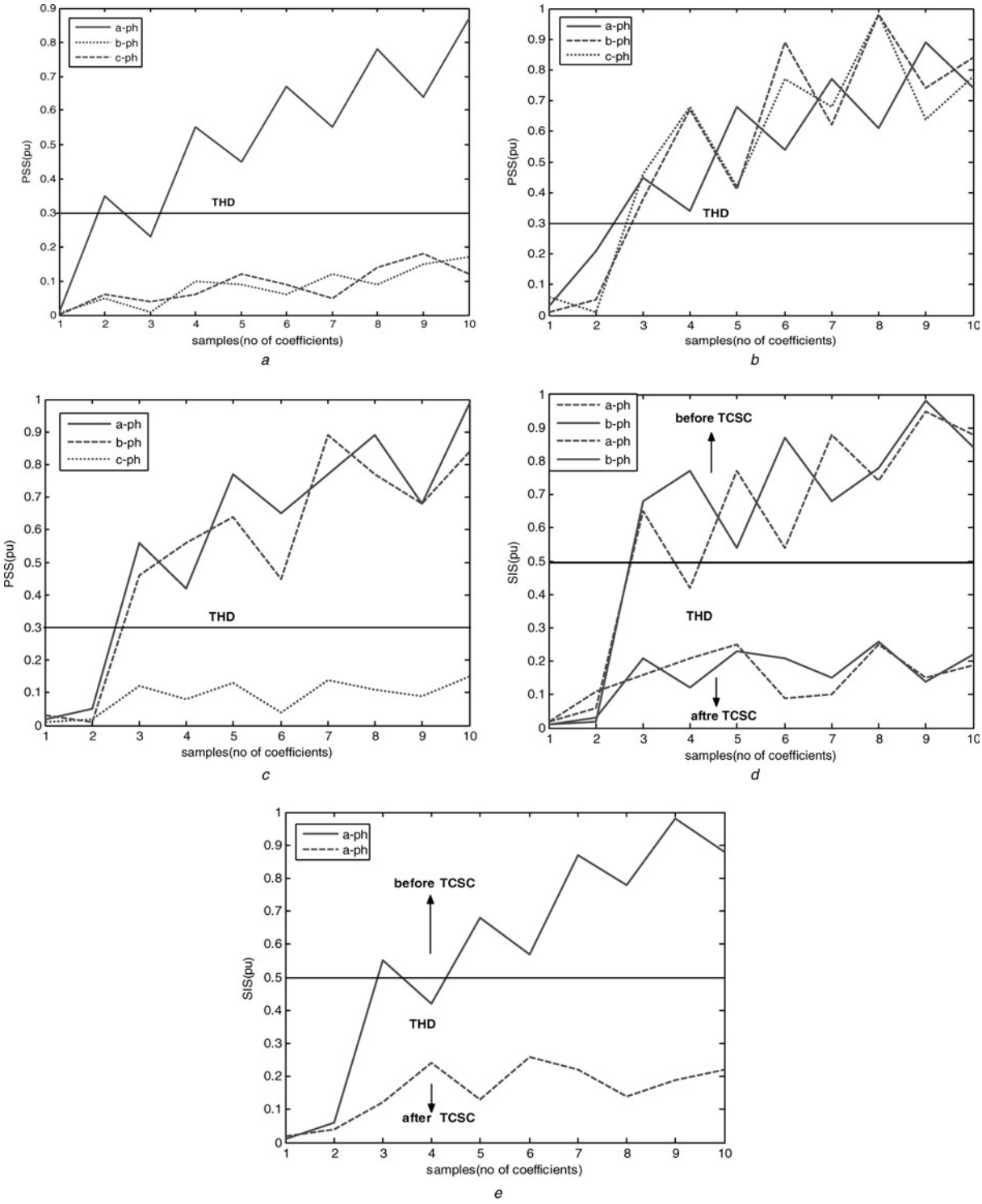

Fig. 9 *Physical transmission line model with TCSC*

a PSS for a–g fault at 40% of the line
b PSS for abc–g fault at 70% of the line
c PSS for ab–g fault at 80% of the line
d SIS for 'ab–g' fault at 25% (before TCSC) and 65% (after TCSC)
e SIS for 'a–g' fault at 35% (before TCSC) and 85% (after TCSC)

shows the SIS for 'ab–g' fault at 15% (before TCSC) and 85% (after TCSC) of the line, $\alpha = 60^\circ$, $R_f = 100\ \Omega$ and Fig. 8*f* SIS for 'ab' fault at 35% (before TCSC) and 75% (after TCSC) of the line, $\alpha = 30^\circ$, $R_f = 150\ \Omega$.

From the results, the faulty section is clearly distinguished for TCSC-based line. It is seen that the SIS in case of faults with TCSC (after TCSC), is below the THD as it is the function of both fundamental and other harmonic components, and harmonic components are highly pronounced in case of faults with TCSC. Thus, the difference between fundamental and other harmonic components results SIS signal much below the THD. But, in the case of faults without TCSC (before TCSC), the SIS is above the THD because the harmonic components are less pronounced compared with faults including TCSC and the difference between fundamental and other harmonic components provides SIS above THD. Thus, the proposed WPT algorithm provides accurate results with wide variations in operating the transmission line having TCSC. The PSS finds the faulty phase involved in the fault process within half cycle of fault inception and triggers SIS for the identification of the fault section in transmission line including TCSC. Thus, both faulty phase and faulty section are identified within one cycle of the fault inception. The proposed method involves small amount of computation as the equations for PSS and SIS operate directly on the WPT coefficients at different levels (sub-band frequency components) coefficient by coefficient (sample by sample) and provides PSS and SIS for faulty phase selection and fault section identification, respectively.

4.4 Results from experimental set-up

The proposed algorithm has been tested on a physical transmission line model with TCSC. The transmission line consists of two 100-km equivalent π-sections with same frequency characteristics as 400 kV line up to 500 Hz. Thus the transmission line represents 200-km line with designed TCSC placed at 50% of the line. The line impedance $Z = 5 + j40\ \Omega$ and line-ground capacitance is 1.5 μF. The line is charged with 400 V, 5 kV A synchronous machines at one end and 400 V at the load end. To properly adjust the firing circuit for creating necessary delay, the phase of the voltage across the triac must be detained. This is accomplished by sensing the voltage across the capacitor which is in parallel with the triac. The method of translating this voltage into a signal delay is done in a series of steps. The first stage is to step the voltage down to 10 V using the step-down transformer. This stepped down voltage is then fed to a zero crossing detector. The zero crossing detector circuit then produces a pulse each time that the capacitor voltage makes the transition from positive to negative or negative to positive. The application of the firing signals to reactance compensators in the other phases of the three phase system requires two phase delays. One is of 120° and other is of 240° for phase B and C, respectively. This will ensure the proper firing of all the triacs. The inductance and capacitance chosen are 25 mH and 24 μF, respectively, to provide compensation varying form 30% (minimum) to 40% (maximum).

The three-phase voltage and current are stepped down at the relaying end with potential transformer of 400/10 V and current transformer (CT) of 15/5 A, respectively. Data collected using PCL-208 data acquisition card (DAC) which uses 12-bit successive approximation technique for A/D (analog to digital) conversion. The card is installed with PC (P-4 machine) with a driver software generally written in C++. It has six I/O channels with input voltage range of ±5 V. Data colleted with a sampling frequency of 1.6 kHz.

The results obtained from the experimental set-up are given in Figs. 9*a–e*. Fig. 9*a* shows the PSS for 'a–g' fault at 40% of the line and Fig. 9*b* shows the PSS for 'abc–g' fault at 70% of the line. The PSS is above THD indicating faulty phases involved in the fault process. Similarly, Fig. 9*c* shows PSS for 'ab–g' fault at 80% of the line. The SIS calculated for faulty section identification are depicted in Fig. 9*d*, and *e*. Fig. 9*d* shows SIS for 'ab–g' fault at 25% (before TCSC) and 65% (after TCSC) of the line and Fig. 9*e* shows SIS for 'a–g' fault at 35% (before TCSC) and 85% (after TCSC) of the line. The THD for faulty phase selection (PSS) and fault section identification (SIS) are selected as 0.3 and 0.5, respectively, after verifying for different operating conditions in the experimental set-up. As SIS and PSS are calculated on per unit (pu) system, the selected THD is well suited for TCSC-based line with other network configuration. From the results obtained from Fig. 9, it is clearly seen that the proposed methods provides accurate results for faulty phase selection and fault section identification for physical transmission line model with TCSC.

5 Conclusions

A new approach for the protection of flexible AC transmission line with TCSC using WPT is presented in this paper. The post-fault-current signal is decomposed into different sub-band components, and harmonic groups are found out providing features of the signal at different frequencies. From the features, PSS and SIS are computed for faulty phase selection and fault section identification, respectively. As the wavelet packet is more flexible and provides more information for signal discrimination; it has the advantage over wavelet transform. The proposed method provides accurate results for physical transmission line model with TCSC with different operating conditions. As the proposed method involves small amount of computation, thus resulting very fast and accurate protection measure for TCSC-based transmission line.

6 References

1 Girgis, A.A., Sallama, A.A., and Karim El-din, A.: 'An adaptive protection scheme foe advanced series compensated (ASC) transmission line', *IEEE Trans. Power Deliv.*, 1998, **13**, pp. 414–420
2 Helbing, S.G., and Karady, G.G.: 'Investigations of an advanced form of series compensation', *IEEE Trans. Power Deliv.*, 1994, **9**, (2), pp. 939–946
3 Larsen, E.V., Clark, K., Miske, S.A., and Urbanek, J.: 'Characteristics and rating considerations of thyristor controlled series compensation', *IEEE Trans. Power Deliv.*, 1994, **9**, (2), pp. 992–1000
4 Song, Y.H., Xuan, Q.Y., and Johns, A.T.: 'Protection of scheme for EHV transmission systems with thyristor controlled series compensation using radial basis function neural networks', *Electric Mach. Power Syst.*, 1997, **25**, pp. 553–565
5 Song, Y.H., Johns, A.T., and Xuan, Q.Y.: 'Artificial neural network based protection scheme for controllable series-compensated EHV transmission lines', *IEE Proc., Gener. Transm. Distrib.*, 1996, **143**, (6), pp. 535–540
6 Noroozian, M., Angquist, L., Ghandhari, M., and Anderson, G.: 'Improving power system dynamics by series connected FACTS devices', *IEEE Trans. Power Deliv.*, 1997, **12**, (4), pp. 1635–1641
7 Dash, P.K., Pradhan, A.K., Panda, G., and Liew, A.C.: 'Adaptive relay setting for flexible AC transmission systems (FACTS)', *IEEE Trans. Power Deliv.*, 2000, **15**, (1), pp. 38–43
8 Gouda, M., Salama, M.A., Sultan, M.R., and Chikhani, A.Y.: 'Power quality detection and classification using wavelet-multiresolution signal decomposition', *IEEE Trans. Power Deliv.*, 1999, **14**, (4), pp. 1469–1476

9 Santoso, S., Powers, E.J., and Grady, W.M.: 'Power quality disturbance data compression using wavelet transform methods', *IEEE Trans. Power Deliv.*, 1997, **12**, (3), pp. 1250–1257
10 Yaussef, O.A.S.: 'Online applications of wavelet transform to power system relaying', *IEEE Trans. Power Deliv.*, 2003, **18**, (4), pp. 1158–1165
11 Chanda, D., Kishore, N.K., and Sinha, A.K.: 'A wavelet multi-resolution analysis for location of faults on transmission lines', *Electr. Power Energy Syst.*, 2003, **25**, pp. 59–69
12 Mann, B.J., and Morrison, I.F.: 'Relaying a three phase transmission line with a digital computer', *IEEE Trans. Power Appar. Syst.*, 1971, **90**, (2), pp. 742–750
13 Liao, Y., and Elangovan, S.: 'Fault noise based approach to phase selection using wavelets based feature extraction', *Electr. Mach. Power Syst.*, 1999, **27**, pp. 389–398
14 Yu, I.K., and Song, Y.H.: 'Wavelet transform and neural network approach to developing adaptive single pole auto reclosing schemes for EHV transmission systems', *IEEE Power Eng. Rev.*, 1998, **18**, (11), pp. 62–64
15 Huang, S.J., and Hsieh, C.T.: 'High-impedance fault detection utilizing morlet wavelet transform approach', *IEEE Trans. Power Deliv.*, 1999, **14**, (4), pp. 1401–1410
16 Wickerhauser, M.V.: 'Lectures on wavelet packet algorithm' (St. Louis, MO: Department of Mathematics, Washington University, 1991)
17 Coifman, R.R., and Meyer, Y.: 'Wavelets and their applications' (Jones and Bartlett, 1992)
18 Hamid, E.Y., and Karvasaki, Z.-I: 'Wavelet packet transform for RMS values and power measurements', *IEEE Power Eng. Rev.*, 2001, **21**, (9), pp. 49–51
19 Parameswariah, C., and Cox, M.: 'Frequency characteristics of Wavelets', *IEEE Trans. Power Deliv.*, 2002, **17**, (3), pp. 800–804
20 Li, X., Qu, L., Wen, G., and Li, C.: 'Application of wavelet packet analysis for fault detection in electro-mechanical systems based on torsional vibration measurement', *Mech. Syst. Signal Process.*, 2002, **17**, (6), pp. 1219–1235
21 Liu, B.: 'Selection of wavelet packet basis for rotating machinery fault diagnosis', *J. Sound Vibr.*, 2004, **284**, (3–5), pp. 567–582
22 Villemoes, F.L.: 'Wavelet packets with uniform time-frequency localization', *C. R. Acad. Sci. Paris*, Ser. I 335, 2002 Analyse mathématique Mathematical Analysi, pp. 793–796
23 Paqueta, H.A., Wardb, K.R., and Pitasc, P.: 'Wavelet packets-based digital watermarking for image verifcation and authentication', *Signal Process.*, 2003, **83**, pp. 2117–2132